

# Combating Mode Collapse in GANs via Manifold Entropy Estimation

Haozhe Liu<sup>1,2</sup>, Bing Li<sup>1✉</sup>, Haoqian Wu<sup>3</sup>, Hanbang Liang, Yawen Huang<sup>2</sup>,  
 Yuexiang Li<sup>2✉</sup>, Bernard Ghanem<sup>1</sup>, Yefeng Zheng<sup>2</sup>  
<sup>1</sup>King Abdullah University of Science and Technology,  
<sup>2</sup>Jarvis Lab, Tencent, <sup>3</sup>YouTu Lab, Tencent

{haozhe.liu;bing.li;bernard.ghanem}@kaust.edu.sa;

lianghanbang2019@email.szu.edu.cn ; {linuswu;vicyxli;yawenhuang;yefengzheng}@tencent.com

## Abstract

*Generative Adversarial Networks (GANs) have shown compelling results in various tasks and applications in recent years. However, mode collapse remains a critical problem in GANs. In this paper, we propose a novel training pipeline to address the mode collapse issue of GANs. Different from existing methods, we propose to generalize the discriminator as feature embedding, and maximize the entropy of distributions in the embedding space learned by the discriminator. Specifically, two regularization terms, i.e. Deep Local Linear Embedding (DLLE) and Deep Isometric feature Mapping (DIsoMap), are designed to encourage the discriminator to learn the structural information embedded in the data, such that the embedding space learned by the discriminator can be well formed. Based on the well-learned embedding space supported by the discriminator, a non-parametric entropy estimator is designed to efficiently maximize the entropy of embedding vectors, playing as an approximation of maximizing the entropy of the generated distribution. Through improving the discriminator and maximizing the distance of the most similar samples in the embedding space, our pipeline effectively reduces the mode collapse without sacrificing the quality of generated samples. Extensive experimental results show the effectiveness of our method which outperforms the GAN baseline, MaF-GAN on CelebA (9.13 vs. 12.43 in FID) and surpasses the recent state-of-the-art energy-based model on the ANIME-FACE dataset (2.80 vs. 2.26 in Inception score).*

## 1. Introduction

Generative Adversarial Networks (GANs) have attracted extensive attentions in recent years. Generally speaking, a GAN consists of a generator network and a discriminator network, where the generator is to generate samples to fool

the discriminator, and the discriminator is trained to discriminate real and generated samples. With such adversarial learning, GANs have shown high-fidelity results in various tasks such as image inpainting [42] and photo super-resolution [26]. Nevertheless, GANs suffer from the mode collapse (or training instability) [29, 37], hindering its further development in generative learning community and potential applications.

To alleviate the mode collapse in GANs, many efforts have been devoted into introducing prior knowledge or adding noise on the generator side. For example, the conditional GANs [6, 31, 33] handle the mode collapse via introducing class-level prior knowledge into GANs. By splitting the generated distribution into several sub-distributions, the complexity for image synthesis would be further reduced. As the distributions of different classes are quite different, mode collapse can be mitigated to some extent. However, annotating the image classes is time-consuming and deviates from the unsupervised setting of GAN. Compared to conditional information, adding noise into networks is a more flexible solution against the mode collapse. Specifically, Style-GANs [21, 22] add Gaussian noise to the output of each convolutional layer to increase the variance of the generated samples. Despite the rapid progress of GAN-based approaches, mode collapse remains an unsolved and challenging problem in GANs.

Different from GANs, another kind of generative models, namely Energy-Based Models (EBMs) [11, 14, 25], have shown the remarkable performances in circumventing the mode collapse. These methods have been attracted increasing attention in recent years. Typically, EBMs estimate the density of the target data distribution, and are trained via maximum likelihood. The partition function has to be estimated during the training of EBMs by adopting expensive Langevin dynamics, while the partition function is generally intractable. Consequently, since training EBMs is challenging, EBMs suffer from high computational complexity, and cannot generate images with competitive fidelity.

✉ Corresponding Author

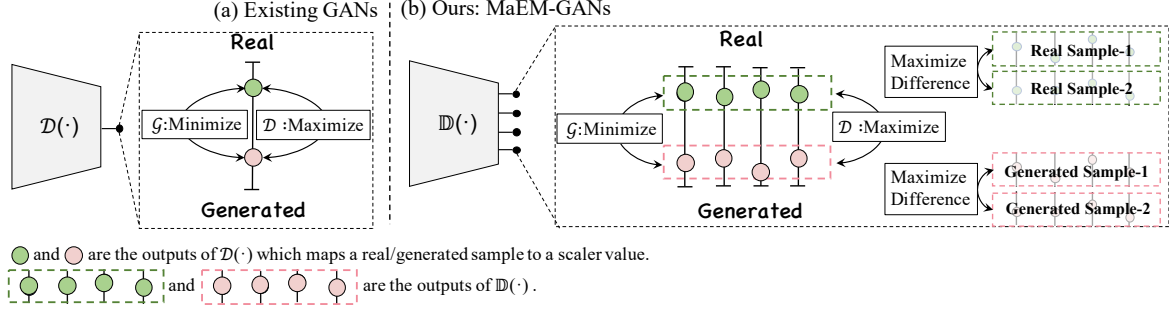


Figure 1. Illustration of our main idea for combating the mode collapse. Different from the existing GANs (a), our MaEM-GANs (b) generalizes the discriminator such that it embeds an image into an  $m$ -dimensional space, instead of just outputting a scalar value. With the embedding vectors of real/generated samples, we maximize the entropy of distributions in the embedding space learned by our discriminator to prevent the mode collapse.

In this paper, inspired by the success of EBMs in avoiding the mode collapse, we propose a novel pipeline named MaEM-GANs (manifold entropy maximization) for training GANs through bridging Wasserstein GANs (WGANs) and EBMs. By analyzing the connection between WGANs and EBMs, we discover that mode collapse in GANs can be avoided by maximizing the entropy of the generated distribution. However, it is nontrivial to directly estimate the entropy of the generated distribution for GANs, especially for large-scale and high-dimension data. Instead, since the discriminator heavily affects the training quality/stability of GANs [20], we propose to address the entropy maximization on the discriminator side. In particular, we propose to generalize the discriminator to feature embedding, such that it embeds images into a lower-dimensional embedding space (see Fig. 1), different from typical GANs. We then maximize the entropy of distributions in the embedding space learned by the discriminator. To further optimize such surrogate objective in an efficient and simple manner, we propose a module named RB-MaEM based on non-parametric entropy estimator using replay buffer. In addition, we propose two regularization terms, namely, Deep Local Linear Embedding (DLLE) and Deep Isometric feature Mapping (DIsoMap), which encourage the discriminator to learn the structural information embedded in the data, such that the embedding space is well formed. Benefited from DLLE and DIsoMap, our method, namely MaEM-GAN, maximizes the entropy in the well-learned embedding space to combat the mode collapse in GANs. Experimental results show that the proposed MaEM-GAN outperforms the recent advanced GAN method MaF-GAN [27] on CelebA (9.13 vs. 12.43 in FID) and surpasses the recent state-of-the-art EBM [11] on the ANIMEFACE dataset (2.80 vs. 2.26 in Inception score).

Our contributions are summarized as follows:

- We propose a novel training pipeline to address the mode collapse issue in GANs, which effectively al-

leviates mode collapse without sacrificing the image quality of generated images.

- We show that the mode collapse in GANs can be reduced by generalizing discriminator as feature embedding and maximizing the entropy of distributions in the embedding space learned by the discriminator.
- The proposed regularization terms, DLLE and DIsoMap, effectively encourage the embedding space of the discriminator to preserve the manifold structure of the data.
- Extensive experiments show that our method achieves superior performances in terms of diversity and image quality on various image generation tasks, compared with both state-of-the-art GANs and EBMs.

## 2. Related Works

**Generative Adversarial Networks.** To overcome the mode collapse, numerous GANs methods have been proposed, such as introducing class-level information [1, 6, 31, 33] or adding noises to different layers [21, 22]. However, these methods need additional annotation, which deviates from the unsupervised setting of GAN, or introduce complex network architecture. Differently, WGANs [2, 15] re-designed the learning objective, where the discriminator performs regression, rather than classification. By dynamically modelling the distance between the generated and real distributions, WGANs can reduce the risk for local minima and mitigate the mode collapse to certain extent. More recently, Realness GANs [40] and Manifold-preserved GANs [27] generalize GANs into a high-dimensional form by mapping the output of the discriminator into a vector to enhance the realness. Since the fidelity of the given image can be judged from different views like ensemble learning, the generator can synthesize images with different attributes to fit the discriminator. The above works indicate

that the discriminator is critical for GANs and can be a potential target to combat mode collapse. Motivated by these progresses [3, 27, 40] with regard to the discriminator, we propose a new pipeline, focusing on designing the simple yet effective constraints on the discriminator side to prevent the mode collapse. Different from the previous methods, we explore how to maximize the entropy of distribution in the embedding space supported by the discriminator, and how to well learn the embedding space. The empirical and theoretical study pointed out that the learning objective of GANs might neglect an intractable entropy term for maximum likelihood, which plays as a key point towards the mode collapse and can be effectively tackled by high-dimensional GANs. Manifold-preserved GAN [27] is the most similar work to ours; however, it neglects the entropy term.

**Energy-based Models.** There has been a rich history for EBM, which can be traced back to Hopfield networks [19] and Boltzmann machines [17]. However, learning an EBM is difficult, since the partition function (*a.k.a.* normalization constant) is intractable and hard to estimate [11]. A common solution is based on expensive Markov Chain Monte Carlo (MCMC) sampling by generally adopting Langevin dynamics [10, 41] and Gibbs sampling [7, 9] to estimate the partition function. Some strict requirements, including parameter tuning [13], early stopping of MCMC [32], and avoiding the use of modern deep modules (*e.g.*, self-attention, dropout and batch/layer normalization) [13], are adopted to mitigate the training instability issue caused by MCMC. These hard requirements limit the capacity of the deep model and might reduce its applicability to some large-scale datasets. More recently, an MCMC-free EBM training strategy [14] was proposed, where a generator is employed as a sampler to achieve amortised training of EBM. In particular, the output of the discriminator (also regarded as EBM) is a single scalar, hence, it is hard to directly estimate the entropy, resulting in complicated processing based on variational inference [14] or Jacobi-determinant [11]. Inspired by the amortised training strategy, we generalize WGAN into a manifold representation and adopt a replay buffer strategy to directly estimate the entropy of the manifold representation. Compared with the state-of-the-art EBMs, the proposed method is simple but effective to estimate entropy, leading to stronger diversity and fidelity on image generation.

### 3. Method

The purpose of our method is to combat the mode collapse in GANs. To this end, we first bridge WGANs and EBMs, since EBMs have shown remarkable performance in avoiding the mode collapse. By analyzing the connections between WGANs and EBMs, we discover that mode collapse in GANs can be prevented via maximizing the entropy

of the generated distribution. However, it is nontrivial to directly estimate the entropy of the generated distribution. Instead, we propose a new training pipeline MaEM-GANs to approximate this objective. In particular, we generalize the discriminator to feature embedding, to embed images into a low-dimensional space. With the generalized discriminator, we propose a surrogate objective to maximize the entropy of the distribution in the embedding space learned by the discriminator. A module RB-MaEM is proposed to efficiently optimize the surrogate objective. Furthermore, we design two manifold regularization terms, *i.e.* Deep Local Linear Embedding (DLLE) and Deep Isometric feature Mapping (DIsomap), to ensure that the embedding space is well-formed and captures the underlying manifold embedded in the high-dimensional data.

#### 3.1. Problem Definition

Inspired by [11, 14], we revisit EBMs and WGANs. By analyzing the connections between them, we discover that the mode collapse can be prevented by maximizing the entropy of the generated distribution.

**Definition 1.** An EBM can be represented from Gibbs density:

$$p_{\theta}(x) = \frac{e^{f_{\theta}(x)}}{Z(\theta)}, \quad (1)$$

where  $f_{\theta} : \mathbb{R}^{h \times w} \rightarrow \mathbb{R}^1$  ( $h$  and  $w$  denote the height and width of the image, respectively) and  $Z(\theta) = \int e^{f_{\theta}(x)} dx$  ( $Z(\theta)$  is the partition function or normalizing constant). EBMs are trained by maximum likelihood estimation:

$$\mathcal{L}_{ebm}(\theta) := -\mathbb{E}_{x \sim \mathcal{P}_r} [\log(\frac{e^{f_{\theta}(x)}}{Z(\theta)})] = -\mathbb{E}_{x \sim \mathcal{P}_r} [f_{\theta}(x)] + \log Z(\theta), \quad (2)$$

where  $\mathcal{P}_r$  is the data distribution.

**Definition 2.** The loss function of WGANs can be defined as

$$\mathcal{L}_{wgan}(\theta) := \mathbb{E}_{x \sim \mathcal{P}_g} [\mathcal{D}(x)] - \mathbb{E}_{x \sim \mathcal{P}_r} [\mathcal{D}(x)], \quad (3)$$

where  $\mathcal{P}_g$  is the generated distribution. Concretely, the discriminator  $\mathcal{D}(\cdot)$  is trained by minimizing  $\mathcal{L}_{wgan}(\theta)$ , while the generator  $\mathcal{G}(\cdot)$  is driven to maximize  $\mathcal{L}_{wgan}(\theta)$ .

**Proposition 1.**  $\mathcal{L}_{wgan}(\theta)$  acts as a lower bound of  $\mathcal{L}_{ebm}(\theta)$  by maximizing the entropy of the generated distribution  $\mathcal{H}(\mathcal{P}_g)$ .

**Proof:** Given the probability density function  $q(x)$  of  $\mathcal{P}_g$  as input, an inequality can be derived as

$$\log Z(\theta) \geq \log Z(\theta) - \text{KL}(q(x) || p_{\theta}(x)), \quad (4)$$

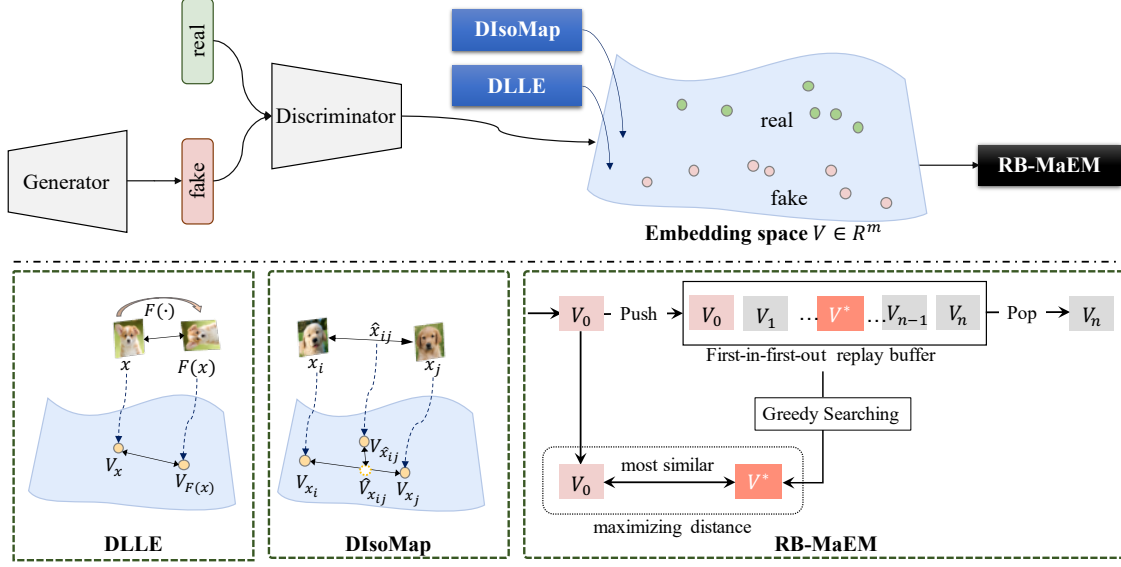


Figure 2. The pipeline of the proposed MaEM-GANs. Our discriminator embeds an input into an  $m$ -dimensional code  $V$ , instead of a scalar value. To preserve the structural information of manifolds embedded in the input data, we design two regularization terms Deep Local Linear Embedding (DLLE) and Deep Isometric feature Mapping (DisoMap). Within the embedding space learned by the discriminator, a replay buffer based non-parametric entropy estimator (RB-MaEM) is proposed to maximize the entropy of distributions by maximizing the distance of most similar samples in the replay buffer.

where  $\text{KL}(\cdot||\cdot)$  denotes the KL-divergence. With respect to  $p_\theta(x) = e^{f_\theta(x)} / Z(\theta)$ ,  $\log Z(\theta)$  can be re-written as

$$\begin{aligned} \log Z(\theta) &\geq \log Z(\theta) + \int_x q(x) \log \left( \frac{e^{f_\theta(x)}}{Z(\theta)q(x)} \right) \\ &= \mathbb{E}_{x \sim \mathcal{P}_g} [f_\theta(x)] + H(\mathcal{P}_g), \end{aligned} \quad (5)$$

where  $H(\mathcal{P}_g)$  is the entropy of  $\mathcal{P}_g$ . Note that model  $f_\theta(x)$  in EBM is equivalent to  $\mathcal{D}(\cdot)$  in GANs. Hence, the connection between  $\mathcal{L}_{wgan}$  and  $\mathcal{L}_{ebm}$  can be established as

$$\begin{aligned} \mathcal{L}_{ebm}(\theta) &= -\mathbb{E}_{x \sim \mathcal{P}_r} [f_\theta(x)] + \log Z(\theta) \\ &\geq \mathcal{L}_{wgan}(\theta) + H(\mathcal{P}_g) \end{aligned} \quad (6)$$

Based on Eq. (6),  $\mathcal{L}_{ebm}(\theta)$  is the upper bound of  $\mathcal{L}_{wgan}(\theta)$  and an entropy term  $H(\mathcal{P}_g)$ . Generally, such an upper bound is very tight, because of the distance between  $\mathcal{L}_{wgan}(\theta) + H(\mathcal{P}_g)$  and  $\mathcal{L}_{ebm}(\theta)$  is the KL-divergence term  $\text{KL}(q(x)||p_\theta(x))$  [14] (see Eq. (4)). That is, for the generator, we can maximize  $\mathcal{L}_{wgan}$  and the entropy term  $H(\mathcal{P}_g)$  to approximate  $\mathcal{L}_{ebm}$  that well alleviates the mode collapse issue. Intuitively,  $H(\mathcal{P}_g)$  plays a key role to tackle the mode collapse problem, which is generally neglected by existing GANs. Therefore, mode collapse can be prevented by maximizing  $H(\mathcal{P}_g)$  of WGANs with the maximum likelihood.

### 3.2. Manifold Representation for WGANs

As discussed above, mode collapse can be prevented by maximizing the entropy of the generated distribution. How-

ever, directly estimating the entropy  $H(\mathcal{P}_g)$  of the generated distribution is intractable, due to the large quantity and high dimensionality of data samples. We address the above problem on the discriminator side, motivated by the fact the discriminator heavily affects the training stability of GANs [20]. Specifically, we propose to generalize the discriminator from the perspective of manifold, and maximize the entropy of distributions in the embedding space supported by the discriminator.

Typical GANs [2, 12, 15] treat the discriminator as a classifier, which classifies an image  $x$  as real or fake according to a scalar value  $\mathcal{D}(x)$ . Different from the scalar-based discriminators, our generalized discriminator  $\mathbb{D}(\cdot)$  learns a mapping which transforms an input image to an  $m$ -dimensional embedding space:  $\mathbb{D}(\cdot) : \mathbf{R}^{h \times w} \rightarrow \mathbf{R}^m$ , where  $h$  and  $w$  are the height and weight of an image  $x$ , respectively, and  $m \geq 1$ .

The embedding space  $\mathbb{D}(\cdot)$  is expected to capture informative characteristics of images. In other words, each dimension of the embedding space  $\mathbb{D}(\cdot)$  corresponds to a critical attribute of images, such as color, texture and structure. Thus, compared with the scalar-based discriminators, our generalized discriminator  $\mathbb{D}$  can provide a more comprehensive representation for the data.

With our generalized discriminator  $\mathbb{D}$ , we reformulate the learning objective of WGANs in Eq. (3). Although the output of our discriminator  $\mathbb{D}$  is a vector, our discriminator determines whether an image  $x$  is real/fake according to the



average value of  $\mathbb{D}(x)$ . The new objective function  $\mathcal{L}_{MaF}$  can be formulated as:

$$\mathcal{L}_{MaF} \triangleq \mathbb{E}_{z \sim \mathcal{P}_z} \left[ \frac{1}{m} \sum_k \mathbb{D}_k(\mathcal{G}(z)) \right] - \mathbb{E}_{x \sim \mathcal{P}_r} \left[ \frac{1}{m} \sum_k \mathbb{D}_k(x) \right], \quad (7)$$

where the standard normal distribution  $\mathcal{N}(0, 1)$  is used for  $p_z$  and  $\frac{1}{m} \sum_k \mathbb{D}_k(x)$  indicates the realness of  $x$ .

### 3.3. Replay Buffer based Manifold Entropy Estimation

With our generalized discriminator  $\mathbb{D}(\cdot)$ , we design a surrogate objective to maximize the entropy of distributions in the embedding space supported by  $\mathbb{D}(\cdot)$ .

Given the  $i^{th}$  image  $x_i$ , we represent it as an embedding code  $V_i = \mathbb{D}(x_i)$  using our discriminator. With such representation, we aim to maximize the entropy of the embedding codes  $\{V_i\}$ 's distribution. Inspired by non-parametric entropy estimator [5], our insight is that if the distance between neighboring samples is maximized in a manifold, the data points in such a manifold will follow a uniform distribution, which maximizes the entropy of data distributions. We hence propose a Replay Buffer based Manifold Entropy Estimation (RB-MaEM) module to efficiently conduct this objective using replay buffer. As shown in Fig. 2, RB-MaEM employs a first-in-first-out replay buffer  $\mathcal{R}$  to store embedded codes  $\{V_0, \dots, V_n\}$  of  $n + 1$  sample images, where  $V_0$  is the code of the  $0^{th}$  image lying at the head of  $\mathcal{R}$  and  $V_n$  is the last code at the tail of  $\mathcal{R}$ . We then search for an embedding code  $V^*$  which is the most similar to  $V_0$  from  $V_1, \dots, V_n$  in buffer  $\mathcal{R}$  with a greed approach. With  $V^*$ , we maximize the entropy of the distribution by maximizing the distance of  $V_0$  and its most similar code  $V^*$ :

$$\mathcal{L}_{ent} = \frac{V_0 \cdot V^*}{\|V_0\| \cdot \|V^*\|} + \lambda \|V_0\|, \quad (8)$$

where  $V^* = \arg \max_{V_i \in \mathcal{R}} \left( \frac{V_0 \cdot V_i}{\|V_0\| \|V_i\|} \right)$  obtained via greedy searching based on cosine similarity, and  $\lambda \|V_0\|$  is a regularization term to ensure the stabilization of the discriminator.

### 3.4. Manifold Regularization

The performance of the proposed RB-MaEM depends on the quality of the embedding space learned by  $\mathbb{D}(\cdot)$ . To ensure that the embedding space captures underlying manifolds embedded in the high-dimensional data, we propose DLLE and DIsoMap to regularize the learning of  $\mathbb{D}$ .

**DLLE.** The first regularization term DLLE enforces the discriminator  $\mathbb{D}$  to preserve nonlinear structure of high-dimensional data by using the local symmetries of linear reconstructions. In particular, DLLE is established upon a simple geometric intuition [35], *i.e.*, a data sample and its

neighbors lie on or are close to a locally linear region of the manifold learned by  $\mathbb{D}(\cdot)$ . Inspired by self-supervised representation learning [8], we characterize a different view of  $x$  as the neighbor of  $x$ . Then, the learning objective  $\mathcal{L}_{LLE}$  of DLLE enforces  $x$  and its neighbor to be similar in the embedding space of  $\mathbb{D}(\cdot)$ :

$$\mathcal{L}_{LLE} \triangleq \mathbb{E}_{x \sim \mathcal{P}_r, \mathcal{P}_g} [\|\mathbb{D}(\mathcal{F}(x)) - \mathbb{D}(x)\|_2] \quad (9)$$

$$= \mathbb{E}_{x \sim \mathcal{P}_r, \mathcal{P}_g} [\|V_{\mathcal{F}(x)} - V_x\|_2], \quad (10)$$

where  $\mathcal{F}(\cdot)$  is the image transformation, such as rotation, adding Gaussian noise and adversarial noise. By capturing the invariance between  $x$  and its neighbors, our DLLE helps the embedding space of  $\mathbb{D}(\cdot)$  preserve the local geometry in the original data, leading to meaningful representations.

**DIsoMap.** The proposed DLLE constrains the learning of embedding space via local positive samples. On the other hand, we propose DIsoMap to exploit the topological structure of different samples for manifold learning. Traditional IsoMap [4] preserves the topological structure information of the data through pairwise distances of data points. Nevertheless, IsoMap yields  $O(N^2)$  complexity, which is computationally prohibitive to directly use it to learn  $\mathbb{D}(\cdot)$  in high-dimensional data (*e.g.*, images). Instead, our DIsoMap estimates the inter-sample distance using the convex combination of different samples, which can be simply calculated and used to train  $\mathbb{D}(\cdot)$  within a mini-batch. Specifically, given two samples  $x_i$  and  $x_j$ , their convex combination  $\hat{x}_{ij}$  in the high-dimensional data space can be defined as

$$\hat{x}_{ij} = \Delta_\delta(x_i, x_j) \triangleq \delta x_i + (1 - \delta)x_j, \quad (11)$$

where  $\delta$  is a random variable sampled from a uniform distribution on  $[0, 1]$ .

To facilitate the manifold learning for  $\mathbb{D}(\cdot)$ , the learning objective of our DIsoMap encourages the embedding space of  $\mathbb{D}(\cdot)$  to preserve the relationship among  $\hat{x}_{ij}$  and data samples  $\{x_i, x_j\}$ :

$$\mathcal{L}_{Iso} = \psi(V_{\hat{x}_{ij}}, \hat{V}_{x_{ij}}) = \frac{V_{\hat{x}_{ij}} \cdot \hat{V}_{x_{ij}}}{\|V_{\hat{x}_{ij}}\| \|\hat{V}_{x_{ij}}\|} \quad (12)$$

where  $V_{\hat{x}_{ij}}$  is the embedding vector of the data-space combination  $\hat{x}_{ij}$  using  $\mathbb{D}(\cdot)$ ,  $\hat{V}_{x_{ij}}$  is the convex combination of  $\{x_i, x_j\}$  in the embedding space via  $\Delta_\delta(\cdot)$  of Eq. (11), *i.e.*  $\hat{V}_{x_{ij}} = \Delta_\delta(\mathbb{D}(x_i), \mathbb{D}(x_j))$ , and  $\psi(\cdot, \cdot)$  is a similarity metric function. Here, we adopt the cosine similarity for  $\psi(\cdot, \cdot)$ . We further use  $\|V_{\hat{x}_{ij}}\| \|\hat{V}_{x_{ij}}\|$  as a normalization term in Eq. (12) to dynamically stabilize the training.

Note that our DIsoMap does not need the expensive graph based estimation adopted in the traditional IsoMap. The proposed method is summarized in Alg. 1.

---

**Algorithm 1** The proposed MaEM-GANs

---

**Input:**

Generator  $\mathcal{G}(\cdot)$ ; Discriminator  $\mathbb{D}(\cdot)$ ; The number of critic iterations  $n_c$ ; Replay buffer  $R_r$  for real samples; and replay buffer  $R_g$  for generated samples.

**Output:**

Trained  $\mathcal{G}(\cdot)$  and  $\mathbb{D}(\cdot)$ ;

```
1: while  $\mathcal{G}(\cdot)$  has not converged do
2:   for  $t = 1$  to  $n_c$  do
3:     Sample  $x_r \sim p_r, z \sim P_z$ ;
4:      $x_g \leftarrow \mathcal{G}(z); \hat{x} \leftarrow \Delta_\delta(x_i, x_j)$ ;
5:      $V_{x_g} \leftarrow \mathbb{D}(x_g); V_{x_r} \leftarrow \mathbb{D}(x_r); V_{\hat{x}} \leftarrow \mathbb{D}(\hat{x})$ ;
6:      $\mathcal{L}_{MaF} \leftarrow \frac{1}{m} \sum_m V_{x_r} - \frac{1}{m} \sum_m V_{x_g}$ ;
7:      $\mathcal{L}_{LLE} \leftarrow \|\mathbb{D}(\mathcal{F}(x_r)) - V_{x_r}\|_2$ ;
8:      $\mathcal{L}_{LLE} += \|\mathbb{D}(\mathcal{F}(x_g)) - V_{x_g}\|_2$ ;
9:      $\mathcal{L}_{Iso} \leftarrow \text{Cosine-Similarity}(V_{\hat{x}}, \Delta_\delta(V_{x_i}, V_{x_j}))$ ;
10:    Greedily search  $R_r$  to obtain  $V^*$ ;
11:     $\mathcal{L}_{ent} \leftarrow \text{Cosine-Similarity}(V_r, V^*)$ ;
12:     $\mathcal{L}_{sum} \leftarrow \mathcal{L}_{MaF} + \mathcal{L}_{LLE} + \mathcal{L}_{Iso} + \sigma \mathcal{L}_{ent}$ ;
13:     $\gamma_t \leftarrow \text{Adam}(\frac{\partial(\mathcal{L}_{sum})}{\partial \gamma_{t-1}})$ ;
14:    Update  $\mathcal{R}_r$ ;
15:  end for
16:   $V_g \leftarrow \mathbb{D}(\mathcal{G}(z))$ ;
17:  Greedily search  $R_g$  to obtain  $V^*$ ;
18:   $\mathcal{L}_{sum} \leftarrow \frac{1}{m} \sum V_g - \sigma \text{Cosine-Similarity}(V_g, V^*)$ ;
19:   $\theta \leftarrow \text{Adam}(-\frac{\partial \mathcal{L}_{sum}}{\partial \theta})$ ;
20:  Update  $\mathcal{R}_g$ ;
21: end while
```

---

## 4. Experimental Results and Analysis

We implement our MaEM-GAN using the public PyTorch toolbox on eight NVIDIA V100 GPUs. To evaluate the performance of the proposed method, extensive experiments are carried on four publicly available datasets with different image sizes, including **CIFAR-10** ( $32 \times 32$  pixels) [23], **ANIMEFACE** ( $64 \times 64$ ), **CelebA** ( $256 \times 256$ ) [28], and **FFHQ** ( $1024 \times 1024$ ) [21]. All the experimental settings, such as optimizer, network architecture and learning rate, are identical to the public benchmarks [11, 21, 27, 40]. Detailed information on the implementation of our MaEM-GAN can be found in *Supplementary Materials*.

**Evaluation metrics.** We use Fréchet Inception Distance (FID) [16] and Inception Score (IS) [36] to evaluate the quality of generated images. Following state-of-the-art approaches [11, 40], we use FID as our main evaluation metric.

To evaluate the effectiveness of our method on alleviat-

<https://www.cs.toronto.edu/~kriz/cifar.html>  
<https://www.kaggle.com/splcher/animefacedataset>  
<https://mmlab.ie.cuhk.edu.hk/projects/CelebA.html>  
<https://github.com/NVlabs/ffhq-dataset>

Table 1. The ablation study of the proposed method on CIFAR-10 in terms of FID  $\downarrow$ .

Baseline	DIsoMap	DLLE	RB-MaEM	FID
✓	×	×	×	>100
✓	✓	×	×	51.96
✓	✓	✓	×	31.70
✓	✓	×	✓	30.73
✓	✓	✓	✓	<b>29.22</b>

Table 2. FID  $\downarrow$  of the proposed method with different image transformation strategies  $\mathcal{F}(\cdot)$  of DLLE on CIFAR-10. (Adv.–Adversarial; Rot.–Rotation; Gau.–Gaussian)

w/ DLLE	Adv. Noise	Rot. and Gau. Noise	FID
✓	×	×	30.73
✓	✓	×	33.04
✓	×	✓	<b>29.22</b>

ing the mode collapse of GANs, we introduce  $F_8$  and a new metric named *I-Variance*, which measures the diversity of generated images to represent the degree of mode collapse. In other words, larger diversity of the generated images indicates lower degree of mode collapse. Hence, I-Variance is defined as the standard deviation of generated distributions, where a generated image is represented by the extracted feature using Inception-V3 [38]:

$$\text{I-Variance} \triangleq \sqrt{\frac{\mathbb{E}_{x \in \mathcal{P}_g} [\|\mathcal{T}(x) - \frac{1}{|\mathcal{P}_g|} \sum_{x \in \mathcal{P}_g} \mathcal{T}(x)\|_2^2]}{|\mathcal{P}_g|}}, \quad (13)$$

where  $\mathcal{T}(\cdot)$  is the Inception-V3 pre-trained on ImageNet. In all experiments, 50,000 images are randomly sampled to calculate FID, IS and I-Variance.

### 4.1. Ablation Studies and Analysis

**Ablation studies.** To conduct ablation studies, we remove DIsoMap, DLLE and RB-MaEM from our method to establish a baseline, *i.e.* a high-dimensional WGAN with  $\mathcal{L}_{MaF}$ . Without our proposed components, the performance of this baseline is unsatisfactory in terms of FID score, as listed in Table 1. More specifically, the discriminator and generator of the baseline with high dimension are trained in an imbalanced mode, which makes the training process unstable. In contrast, the performance of our method is significantly improved by adding each proposed component into the baseline, validating the effectiveness of our components. As shown in Table 1, DIsoMap is the key component to stabilize the training process, since this term can dynamically ensure the distance between the real and generated distributions to be tractable. Hence, DIsoMap drives the baseline to achieve an FID of 51.96. However, this term might lead to a trivial solution, *i.e.* each dimension outputs the same value. To overcome the issue, DLLE and RB-MaEM are added

Table 3. The FID scores  $\downarrow$  of the proposed method using different replay buffer sizes on CIFAR-10.

Buffer size	128	512	1024	2048
FID	31.58	32.36	<b>29.22</b>	31.87

Table 4. The I-Variance score  $\uparrow (\times 10^{-3})$  of the proposed method on CIFAR-10. I-Variance score denotes the variance of the class-wise outputs from Inception-V3.

Configuration	CIFAR-10	ANIMEFACE
Baseline	$3.41 \pm 0.03$	$2.46 \pm 0.03$
+ RB-MaEM	<b><math>4.88 \pm 0.04</math></b>	<b><math>2.59 \pm 0.04</math></b>

and help the discriminator yield non-trivial representation, which further improve our performance to 31.70 and 30.73 in FID, respectively. By incorporating all proposed components, our method achieves the best FID score of 29.22.

**Impact of Hyper-parameters.** For DLLE, Tab. 2 investigates different strategies of generating the neighbors of a given sample, where the first strategy adds the adversarial perturbation into the image. The second strategy employs image augmentations *i.e.* rotation and adding Gaussian noises, which is simpler yet achieves better performance in FID than the first one. In addition, Table 3 lists our results using different buffer size. Our method would be degraded, if the buff size is too small to store enough meaningful samples for maximizing the entropy. When buffer size is 1024, our method achieves the best performance,

**The effectiveness of the discriminator with manifold representation.** In our method, the discriminator yields a vector to measure the realness of generated images. Each element in the vector measures the sample-wise realness from a specific attribute. To demonstrate the effectiveness of manifold representation, we feed 50,000 generated images to our discriminator and obtain the corresponding vectors. Fig. 3 shows the ‘realest’ samples ranked along different elements/dimensions of the obtained vectors. We can observe that the top samples ranked by different dimensions of our discriminator’s output exhibit different attributes such as color and styles. Hence, introducing manifold representation not only is effective to estimate the entropy, but also helps the discriminator to assess the realness from different aspects (like ensemble learning).

**The effectiveness of RB-MaEM on alleviating mode collapse.** We verify the importance of RB-MaEM on alleviating the mode collapse issue by measuring the diversity of generated images, where I-Variance score is adopted to quantitatively assess the diversity of generated images. Table 4 shows that our method without RB-MaEM only achieves I-Variance score of 3.41. In contrast, the I-Variance score increases to 4.88 by adding RB-MaEM. This shows that our RB-MaEM can significantly improve the diversity of generated images and effectively alleviate mode

Table 5. FID  $\downarrow$  and Inception Score  $\uparrow$  of GAN models on CelebA and CIFAR-10. All methods use the same backbone of DCGAN [34] and BigGAN [6].

Model based on DCGAN	CIFAR-10 (FID)	CelebA (FID)
WGAN [2]	55.96	-
HingeGAN [43]	42.40	25.57
LSGAN [30]	42.01	30.76
Std-GAN [12]	38.56	27.02
WGAN-GP [15]	41.86	70.28
Realness GAN-Obj.1 [40]	36.73	-
Realness GAN-Obj.2 [40]	34.59	23.51
Realness GAN-Obj.3 [40]	36.21	-
MaF-CwGAN [27]	39.24	-
MaF-DwGAN [27]	33.73	-
MaF-EwGAN [27]	30.85	12.43
Ours	<b>29.22</b>	<b>9.14</b>
Model based on BigGAN	CIFAR-10 (FID)	CIFAR-10 (IS)
Unconditional BigGAN	16.04	9.10
Unconditional BigGAN + Ours	<b>13.86</b>	<b>9.27</b>

Table 6. FID and IS on ANIMEFACE for different EBMs and diffusion models.

Model	IS $\uparrow$	FID $\downarrow$	$F_8 \uparrow$
WGAN-0GP [39]	2.22	9.76	0.95
MEG [24]	2.20	9.31	0.95
VERA [14]	2.15	41.00	0.52
EBM-0GP [11]	2.26	20.53	0.89
EBM-BB [11]	2.26	12.75	0.94
DDPM* [18]	2.18	8.81	0.94
Ours:	<b>2.80</b>	<b>8.62</b>	<b>0.98</b>

Table 7. FID of StyleGAN-V1/2 and our method on FFHQ.

Model	FID $\downarrow$
StyleGAN-V1 [21]	4.40
StyleGAN-V2 [22]	2.84
StyleGAN-V2 + Ours	<b>2.67</b>

collapse.

## 4.2. Comparison with State-of-the-art Methods

To show the superiority of our method, we compare our method with recent state-of-the-art GAN models and energy-based models. Note that the results of all baseline methods are duplicated from the existing benchmarks [11, 40] without re-implementation.

**Comparison with GAN models.** Table 5 shows the comparison results on CIFAR-10 and CelebA datasets. Compared with state-of-the-arts GAN, our method achieves the best FID score on both datasets. Specifically, MaF-GAN is a recent work most related to ours, which also generalizes WGAN into a high-dimensional form. Our



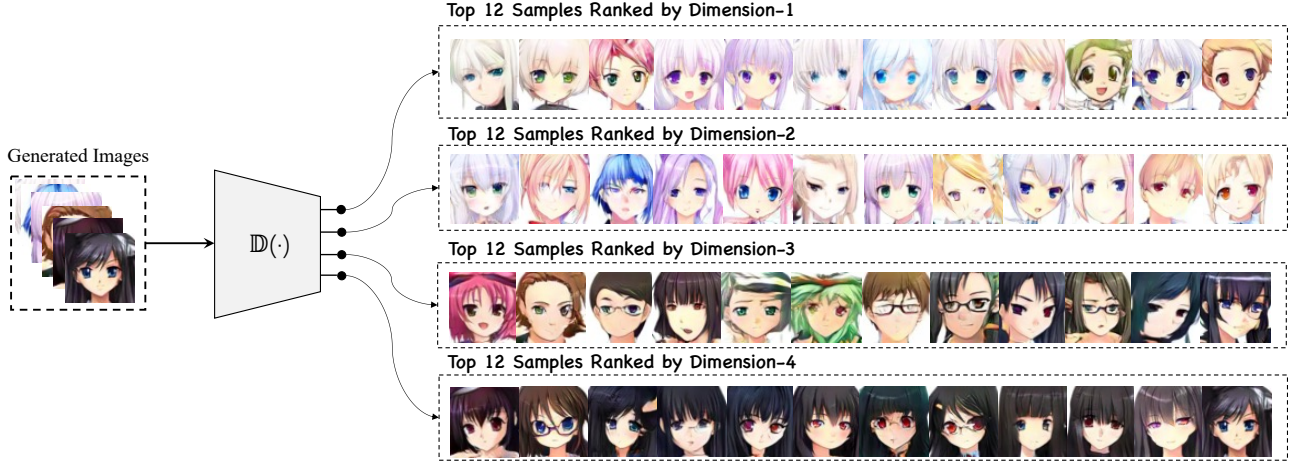


Figure 3. Top five generated images ranked by the individual dimension of the discriminator on ANIMEFACE. In each row, a generated image is ranked according to the  $c^{\text{th}}$  dimension value of its embedded code  $V$  extracted by our discriminator ( $c = 1, 2, 3, 4$ ).

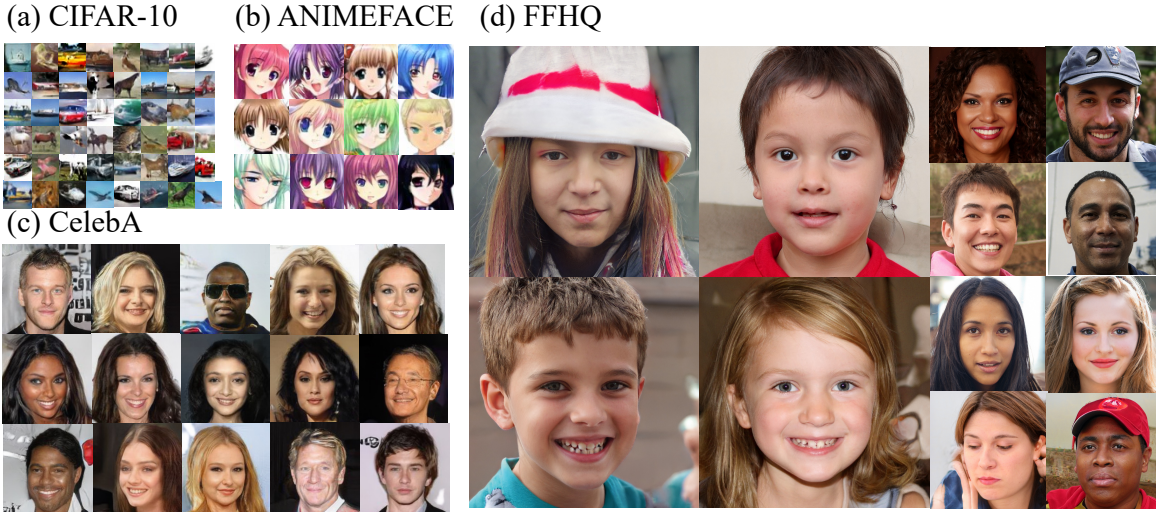


Figure 4. The generated samples of the proposed method on (a) CIFAR-10 ( $32 \times 32$ ), (b) ANIMEFACE ( $64 \times 64$ ), (c) CelebA ( $256 \times 256$ ) and (d) FFHQ ( $1024 \times 1024$ ).

method surpasses MaF-GAN by a large margin, since our method explicitly maximizes the entropy of distribution in the embedding space of the discriminator. Furthermore, we demonstrate that our method facilitates the training of very deep GAN architectures even with complicated training strategies. In particular, our method is incorporated into StyleGAN-V2 [22] and BigGAN [6] by adding the proposed learning objective to their methods. And the consistent improvements can be found in Table 5 and Table 7.

**Comparison with energy-based models.** We compare our method with representative energy-based models, including MEG [24], VERA [14], EBM-0GP [11] and EBM-BB [11]. For a more comprehensive study, we also include WGAN-0GP [39] and Denoising Diffusion Prob-

abilistic Model (DDPM) [18]. DDPM can be regarded as an upper bound for generation performance, since this method generates images by expensive iterative optimization. Following [11], we conduct the experiments on the AnimeFace dataset. Table 6 shows that our method outperforms all energy-based models with the highest IS (2.80) and  $F_8$  (0.98), and lowest FID (8.62), demonstrating that our method not only ensures the fidelity of the generated images, but also significantly improves their diversity.

## 5. Conclusion

In this paper, we proposed a novel method to alleviate mode collapse in GANs. Our method generalizes the



discriminator as a feature embedder, and mode collapse in GANs can be alleviated by maximizing the entropy of distributions in the embedding space learned by the discriminator. Two manifold regularization terms were proposed to preserve the information in the manifold embedded in the data. Based on the well-learned embedding space, a replay-buffer-based entropy estimator was proposed to maximize the diversity of samples in the embedding space. Through improving the discriminator and maximizing the entropy of distributions in the embedding space, our method effectively reduces the mode collapse without sacrificing the quality of generated samples. Extensive experiments showed the superior performance of our method on various datasets.

## References

- [1] Dongsheng An, Yang Guo, Na Lei, Zhongxuan Luo, Shing-Tung Yau, and Xianfeng Gu. Ae-ot: a new generative model based on extended semi-discrete optimal transport. In *ICLR*, 2019. [2](#)
- [2] Martin Arjovsky, Soumith Chintala, and Léon Bottou. Wasserstein generative adversarial networks. In *International Conference on Machine Learning*, pages 214–223. PMLR, 2017. [2](#), [4](#), [7](#)
- [3] Han AZhang, Zizhao Zhang, Augustus Odena, and Honglak Lee. Consistency regularization for generative adversarial networks. In *ICLR*, 2020. [3](#)
- [4] Mukund Balasubramanian and Eric L Schwartz. The IsoMap algorithm and topological stability. *Science*, 295(5552):7–7, 2002. [5](#)
- [5] Jan Beirlant, Edward J Dudewicz, László Györfi, Edward C Van der Meulen, et al. Nonparametric entropy estimation: An overview. *International Journal of Mathematical and Statistical Sciences*, 6(1):17–39, 1997. [5](#)
- [6] Andrew Brock, Jeff Donahue, and Karen Simonyan. Large scale GAN training for high fidelity natural image synthesis. *ICLR*, 2019. [1](#), [2](#), [7](#), [8](#)
- [7] Chain Monte Carlo. Markov Chain Monte Carlo and Gibbs sampling. *Lecture notes for EEB*, 581:540, 2004. [3](#)
- [8] Ting Chen, Simon Kornblith, Mohammad Norouzi, and Geoffrey Hinton. A simple framework for contrastive learning of visual representations. In *International Conference on Machine Learning*, pages 1597–1607. PMLR, 2020. [5](#)
- [9] Christopher De Sa, Vincent Chen, and Wing Wong. Mini-batch Gibbs sampling on large graphical models. In *International Conference on Machine Learning*, pages 1173–1181, 2018. [3](#)
- [10] Yilun Du and Igor Mordatch. Implicit generation and modeling with energy based models. *Advances in Neural Information Processing Systems*, 32, 2019. [3](#)
- [11] Cong Geng, Jia Wang, Zhiyong Gao, Jes Frellsen, and Søren Hauberg. Bounds all around: training energy-based models with bidirectional bounds. *Advances in Neural Information Processing Systems*, 34, 2021. [1](#), [2](#), [3](#), [6](#), [7](#), [8](#)
- [12] Ian Goodfellow, Jean Pouget-Abadie, Mehdi Mirza, Bing Xu, David Warde-Farley, Sherjil Ozair, Aaron Courville, and Yoshua Bengio. Generative Adversarial Nets. *Advances in Neural Information Processing Systems*, 27, 2014. [4](#), [7](#)
- [13] Will Grathwohl, Kuan-Chieh Wang, Jörn-Henrik Jacobsen, David Duvenaud, Mohammad Norouzi, and Kevin Swersky. Your classifier is secretly an energy based model and you should treat it like one. *International Conference on Learning Representations*, 2020. [3](#)
- [14] Will Sussman Grathwohl, Jacob Jin Kelly, Milad Hashemi, Mohammad Norouzi, Kevin Swersky, and David Duvenaud. No {mcmc} for me: Amortized sampling for fast and stable training of energy-based models. In *International Conference on Learning Representations*, 2021. [1](#), [3](#), [4](#), [7](#), [8](#)
- [15] Ishaan Gulrajani, Faruk Ahmed, Martin Arjovsky, Vincent Dumoulin, and Aaron C Courville. Improved training of Wasserstein GANs. *Advances in Neural Information Processing Systems*, 30, 2017. [2](#), [4](#), [7](#)
- [16] Martin Heusel, Hubert Ramsauer, Thomas Unterthiner, Bernhard Nessler, and Sepp Hochreiter. GANs trained by a two time-scale update rule converge to a local Nash equilibrium. *Advances in Neural Information Processing Systems*, 30, 2017. [6](#)
- [17] Geoffrey E Hinton and Terrence J Sejnowski. Optimal perceptual inference. In *Proceedings of the IEEE conference on Computer Vision and Pattern Recognition*, volume 448, pages 448–453. Citeseer, 1983. [3](#)
- [18] Jonathan Ho, Ajay Jain, and Pieter Abbeel. Denoising diffusion probabilistic models. *Advances in Neural Information Processing Systems*, 33:6840–6851, 2020. [7](#), [8](#)
- [19] John J Hopfield. Neural networks and physical systems with emergent collective computational abilities. *Proceedings of the National Academy of Sciences*, 79(8):2554–2558, 1982. [3](#)
- [20] Tero Karras, Miika Aittala, Janne Hellsten, Samuli Laine, Jaakko Lehtinen, and Timo Aila. Training generative adversarial networks with limited data. *Advances in Neural Information Processing Systems*, 33:12104–12114, 2020. [2](#), [4](#)
- [21] Tero Karras, Samuli Laine, and Timo Aila. A style-based generator architecture for Generative Adversarial Networks. In *Proceedings of the IEEE/CVF Conference on Computer Vision and Pattern Recognition*, pages 4401–4410, 2019. [1](#), [2](#), [6](#), [7](#)
- [22] Tero Karras, Samuli Laine, Miika Aittala, Janne Hellsten, Jaakko Lehtinen, and Timo Aila. Analyzing and improving the image quality of StyleGAN. In *Proceedings of the IEEE/CVF Conference on Computer Vision and Pattern Recognition*, pages 8110–8119, 2020. [1](#), [2](#), [7](#), [8](#)
- [23] Alex Krizhevsky, Geoffrey Hinton, et al. Learning multiple layers of features from tiny images. 2009. [6](#)
- [24] Rithesh Kumar, Sherjil Ozair, Anirudh Goyal, Aaron Courville, and Yoshua Bengio. Maximum entropy generators for energy-based models. *arXiv preprint arXiv:1901.08508*, 2019. [7](#), [8](#)
- [25] Yann LeCun, Sumit Chopra, Raia Hadsell, M Ranzato, and F Huang. A tutorial on energy-based learning. *Predicting structured data*, 1(0), 2006. [1](#)

- [26] Zhen Li, Jinglei Yang, Zheng Liu, Xiaomin Yang, Gwanggil Jeon, and Wei Wu. Feedback network for image super-resolution. In *Proceedings of the IEEE/CVF conference on computer vision and pattern recognition*, pages 3867–3876, 2019. 1
- [27] Haozhe Liu, Hanbang Liang, Xianxu Hou, Haoqian Wu, Feng Liu, and Linlin Shen. Manifold-preserved GANs. *arXiv preprint arXiv:2109.08955*, 2021. 2, 3, 6, 7
- [28] Ziwei Liu, Ping Luo, Xiaogang Wang, and Xiaoou Tang. Deep learning face attributes in the wild. In *Proceedings of the IEEE International Conference on Computer Vision*, pages 3730–3738, 2015. 6
- [29] Karttikeya Mangalam and Rohin Garg. Overcoming mode collapse with adaptive multi adversarial training. *arXiv preprint arXiv:2112.14406*, 2021. 1
- [30] Xudong Mao, Qing Li, Haoran Xie, Raymond YK Lau, Zhen Wang, and Stephen Paul Smolley. Least squares generative adversarial networks. In *Proceedings of the IEEE International Conference on Computer Vision*, pages 2794–2802, 2017. 7
- [31] Mehdi Mirza and Simon Osindero. Conditional Generative Adversarial Nets. *arXiv preprint arXiv:1411.1784*, 2014. 1, 2
- [32] Erik Nijkamp, Mitch Hill, Song-Chun Zhu, and Ying Nian Wu. Learning non-convergent non-persistent short-run MCMC toward energy-based model. *Advances in Neural Information Processing Systems*, 32, 2019. 3
- [33] Augustus Odena, Christopher Olah, and Jonathon Shlens. Conditional image synthesis with auxiliary classifier GANs. In *International Conference on Machine Learning*, pages 2642–2651. PMLR, 2017. 1, 2
- [34] Alec Radford, Luke Metz, and Soumith Chintala. Unsupervised representation learning with deep convolutional generative adversarial networks. *International Conference on Learning Representations*, 2016. 7
- [35] Sam T Roweis and Lawrence K Saul. Nonlinear dimensionality reduction by locally linear embedding. *science*, 290(5500):2323–2326, 2000. 5
- [36] Tim Salimans, Ian Goodfellow, Wojciech Zaremba, Vicki Cheung, Alec Radford, and Xi Chen. Improved techniques for training GANs. *Advances in Neural Information Processing Systems*, 29, 2016. 6
- [37] Divya Saxena and Jiannong Cao. Generative adversarial networks (GANs) challenges, solutions, and future directions. *ACM Computing Surveys (CSUR)*, 54(3):1–42, 2021. 1
- [38] Christian Szegedy, Vincent Vanhoucke, Sergey Ioffe, Jon Shlens, and Zbigniew Wojna. Rethinking the Inception architecture for computer vision. In *Proceedings of the IEEE Conference on Computer Vision and Pattern Recognition*, pages 2818–2826, 2016. 6
- [39] Hoang Thanh-Tung, Truyen Tran, and Svetha Venkatesh. Improving generalization and stability of generative adversarial networks. *International Conference on Learning Representations*, 2019. 7, 8
- [40] Yuanbo Xiangli, Yubin Deng, Bo Dai, Chen Change Loy, and Dahua Lin. Real or not real, that is the question. *International Conference on Learning Representations*, 2020. 2, 3, 6, 7
- [41] Jianwen Xie, Yang Lu, Ruiqi Gao, Song-Chun Zhu, and Ying Nian Wu. Cooperative training of descriptor and generator networks. *IEEE transactions on pattern analysis and machine intelligence*, 42(1):27–45, 2018. 3
- [42] Jiahui Yu, Zhe Lin, Jimei Yang, Xiaohui Shen, Xin Lu, and Thomas S Huang. Generative image inpainting with contextual attention. In *Proceedings of the IEEE conference on computer vision and pattern recognition*, pages 5505–5514, 2018. 1
- [43] Junbo Zhao, Michael Mathieu, and Yann LeCun. Energy-based generative adversarial network. *International Conference on Learning Representations*, 2017. 7